DOI: 10.1002/cphc.200600598

A Theoretical Study of Surface Reduction Mechanisms of CeO_2(111) and (110) by H_2

Hsin-Tsung Chen,[b] Yong Man Choi,*[a] Meilin Liu,[a] and M. C. Lin*[b, c]

Reaction mechanisms for the interactions between CeO_2(111) and (110) surfaces are investigated using periodic density functional theory (DFT) calculations. Both standard DFT and DFT+U calculations to examine the effect of the localization of Ce 4f states on the redox chemistry of H_2–CeO_2 interactions are described. For mechanistic studies, molecular and dissociative local minima are initially located by placing an H_2 molecule at various active sites of the CeO_2 surfaces. The binding energies of physisorbed species optimized using the DFT and DFT+U methods are very weak. The dissociative adsorption reactions producing hydroxylated surfaces are all exothermic; exothermicities at the DFT level range from 4.1 kcal mol^{-1} for the (111) to 26.5 kcal mol^{-1} for the (110) surface, while those at the DFT+U level are between 65.0 kcal mol^{-1} for the (111) and 81.8 kcal mol^{-1} for the (110) surface. Predicted vibrational frequencies of adsorbed OH and H_2O species on the surfaces are in line with available experimental and theoretical results. Potential energy profiles are constructed by connecting molecularly adsorbed and dissociatively adsorbed intermediates on each CeO_2 surface with tight transition states using the nudged elastic band (NEB) method. It is found that the U correction method plays a significant role in energetics, especially for the intermediates of the exit channels and products that are partially reduced. The surface reduction reaction on CeO_2(110) is energetically much more favorable. Accordingly, oxygen vacancies are more easily formed on the (110) surface than on the (111) surface.

1. Introduction

Ceria (CeO_2) is an important catalyst in various industrial and environmental applications such as a three-way automotive exhaust catalyst (TWC),[1] oxygen storage,[2] the oxidation of hydrocarbons[3] and CO,[4] and the decomposition of alcohols[5] and aldehydes.[6] Moreover, rare-earth-doped CeO_2, such as gadolia-doped ceria (GDC), has also been used as an electrolyte for low-temperature solid oxide fuel cells (SOFCs).[7] To understand the catalytic properties of both pure CeO_2 and metal/CeO_2 materials, it is imperative to examine the redox surface chemistry. Although many studies regarding the defect chemistry of CeO_2 have been conducted,[8] its reduction processes have been scarcely examined. In particular, the defect chemistry of CeO_2 under H_2 atmosphere has been studied by various experimental techniques, such as temperature-programmed reduction (TPR)[9–11] and NMR.[12] On the basis of experimental results obtained by using TPR and temperature programmed desorption mass spectrometry (TPD-MS), Bernal and coworkers[13] reported that H_2–CeO_2 interactions are a surface process rather than the hydroxylation and incorporation of hydrogen into the bulk, as proposed by Bruce and coworkers.[10] Although numerous theoretical investigations on bulk CeO_2, its surfaces (including reduced ceria),[14–20] and the interactions of atomic H with CeO_2(111) and (110)[18] have been reported, to the best of our knowledge, the mechanisms of H_2–CeO_2 interactions have not been adequately addressed. In this study, we report the reduction mechanisms of CeO_2(111) and (110) surfaces by H_2 using periodic density functional theory (DFT) methods. In particular, to properly characterize the electronic structure of CeO_2, the DFT+U method[15,20–23] was applied. Detailed potential-energy surfaces for all low-lying reaction pathways are reported.

Computational Methods

We performed DFT plane-wave calculations using the Vienna ab initio simulation package (VASP)[24] with the projector-augmented wave method (PAW).[25] The exchange–correlation function was treated with the generalized gradient approximation (GGA) of the Perdew–Wang (PW91) functional, which has been shown to work well for bulk and surface properties of CeO_2.[22,26] A 400 eV cut-off energy that allows convergence to be 0.01 eV in the total energy was used. The Brillouin zone was sampled with the (6×6×6) and (6×6×1) Monkhorst–Pack[27] mesh **k**-points for bulk and surface calculations, respectively. To avoid interactions between slabs, all

[a] *Dr. Y. M. Choi, Prof. Dr. M. Liu*
Center for Innovative Fuel Cell and Battery Technologies
School of Materials Science and Engineering
Georgia Institute of Technology, Atlanta, GA 30332 (USA)
Fax: (+1) 404-894-9140
E-mail: yongman.choi@mse.gatech.edu

[b] *Dr. H.-T. Chen, Prof. Dr. M. C. Lin*
Department of Chemistry, Emory University
1515 Dickey Drive, Atlanta, GA 30322 (USA)
Fax: (+1) 404-727-6586
E-mail: chemmcl@emory.edu

[c] *Prof. Dr. M. C. Lin*
Center for Interdisciplinary Molecular Science
National Chiao Tung University, Hsinchu, 30010 (Taiwan)
Fax: (+886) 3-571-2179

Supporting information for this article is available on the WWW under http://www.chemphyschem.org or from the author.

slabs were separated by a vacuum space greater than 15 Å. As depicted in Figure 1a, CeO_2 has a fluorite structure in which each cerium cation is surrounded by eight equivalent oxygen ions, while each oxygen ion is surrounded by a tetrahedron of four

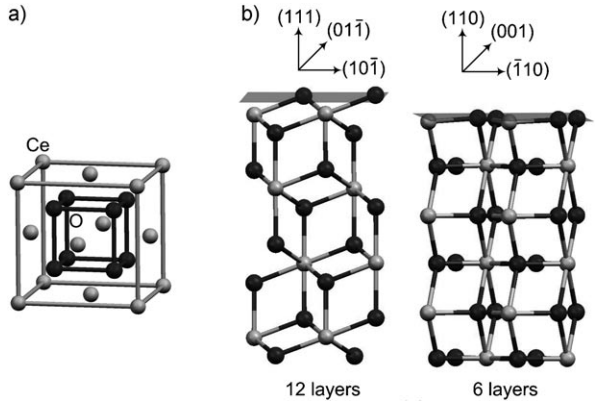

Figure 1. a) The fluorite structure of CeO_2. b) Slab models for cubic CeO_2(111) and (110) surfaces.

equivalent cerium ions.[28] The CeO_2(111) and (110) surfaces were modeled as periodically repeated slabs consisting of twelve and six atomic layers, respectively, which represent p($\sqrt{3}$×1) and p(1×2) lateral cells, respectively (Figure 1b). The bottom six and three atomic layers of the CeO_2(111) and (110) surfaces, respectively, were unrelaxed and set to the estimated bulk parameters, while the remaining layers were fully relaxed. In this study, the DFT and DFT+U methods[29] were performed in order to accurately correct the strong on-site Coulomb repulsion of Ce 4f states on reduced ceria surfaces.[15,20,22,23] For the DFT+U calculations, a series of bulk calculations were carried out by varying the U value from 0.0 to 7.0 eV. As Jiang and coworkers[15] reported, we found the optimal values of U and J are 7.0 and 0.7 eV, respectively. In this study, we calculated adsorption energies according to Equation (1):

$$\Delta E_{ads} = E[\text{slab} + \text{adsorbate}] - (E[\text{slab}] + E[\text{adsorbate}]) \quad (1)$$

where E[slab+adsorbate], E[slab], and E[adsorbate] are the calculated electronic energies of adsorbed species on a ceria surface, a bare ceria surface, and a gas-phase H_2 molecule, respectively. The nudged elastic band (NEB) method[30] was applied to locate transition states, and potential energy surfaces (PESs) were constructed accordingly. All transition states were identified by the number of imaginary frequencies (NIMG) with NIMG=1.

2. Results and Discussion

2.1. Bulk and Clean Surfaces of CeO_2 and Gas-Phase H_2, OH, and H_2O Molecules

To ensure the validity of the surface models displayed in Figure 1b, we first compared our lattice parameters, total density of states, and formation energy of an oxygen vacancy with literature values. As compiled in Table 1, the calculated lattice parameters of bulk CeO_2 using the DFT and DFT+U methods are in very good agreement with the experimental value of 5.411 Å.[33] Shown in Figure 2 is the calculated total density of states for bulk CeO_2. While the calculated energy gaps of O 2p→Ce 4f and O 2p→Ce 5d at the DFT level are 1.8 eV and

Table 1. Experimental and calculated lattice parameters for CeO_2.

Methods	Lattice parameters [Å]
this work	5.419,[a] 5.436[b]
GGA-DFT	5.480,[31] 5.470[16]
LDA-DFT	5.390,[31] 5.370[16]
HF	5.385,[14] 5.546[33]
Experimental	5.411

[a] Calculated at the DFT level. [b] Calculated at the DFT+U level.

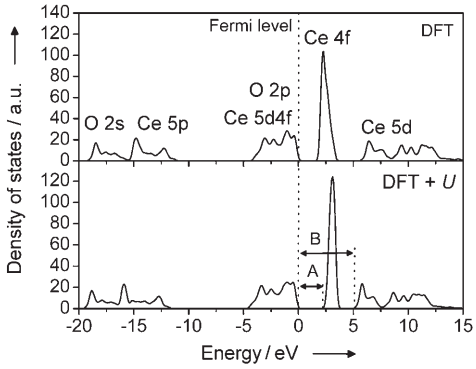

Figure 2. Total density of states of bulk CeO_2 calculated at the DFT and DFT+U levels. A and B correspond to the calculated energy gaps for O 2p→Ce 4f and O 2p→Ce 5d, respectively.

5.5 eV, respectively, those by the DFT+U method with the values of U and J of 7.0 and 0.7 eV, respectively, are 2.3 eV and 5.1 eV (see Table S1 in the Supporting Information). It is known that the O 2p→Ce 5d band gap is less important compared to the O 2p→Ce 4f band gap.[15] Similar to previous studies,[19] the formation energy of an oxygen vacancy within the bulk was also estimated based on the reaction $CeO_2 \rightarrow CeO_{2-x} + 1/2\ O_2(g)$. The vacancy energy from the DFT method is 114.1 kcal mol^{-1}, whereas that from DFT+U is 92.9 kcal mol^{-1}, providing a better agreement with the experimental value of 94.5 kcal mol^{-1}.[34] Shown in Table S2 (see the Supporting Information) are the surface energies of CeO_2(111) and (110) surfaces estimated in units of J m^{-2} according to Equation (2):[19]

$$E_{surf} = \frac{1}{2S}(E_{slab} - E_{bulk}) \quad (2)$$

where E_{surf}, S, E_{slab}, and E_{bulk} represent the surface energy, the surface area, and the calculated electronic energies of the slab and the bulk, respectively. Thus, a lower surface energy corresponds to a more stable surface. As summarized in Table S2, our predicted relaxed surface energies for the (111) and (110) surfaces are 0.60 and 0.96 J m^{-2}, respectively, which are in line with other DFT results.[16,19] In addition, it is consistent with the experimental data by Lyons et al.,[35] who verified that the (111) facet of CeO_2 is the most stable. As Jiang et al.[15] reported, the surface-energy difference calculated by the DFT and DFT+U methods for perfect CeO_2 is negligible. Furthermore, we estimated the adsorption energies of H_2O–CeO_2(111) interactions with various adsorption configurations similar to those of Hen-

derson et al.,[38] as shown in Figure 3, since the experimental data of H_2O–CeO_2 interactions are well-established in the literature.[39] As displayed in Figure 3, our calculated adsorption energies from DFT vary from −4.4 to −11.9 kcal mol^{-1}. Notably,

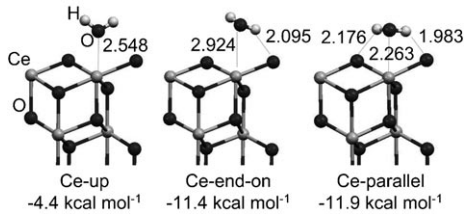

Figure 3. Optimized geometries and adsorption energies for H_2O adsorption on the CeO_2(111) surface at the DFT level.

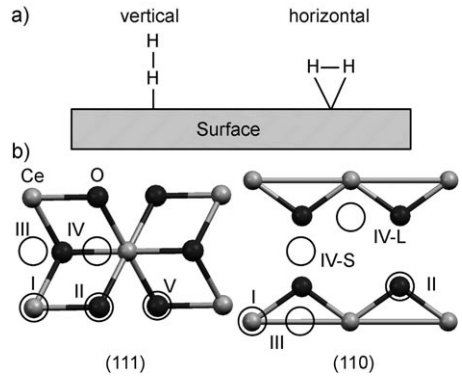

Figure 4. a) Schematics of vertical and horizontal configurations of H_2 on CeO_2 surfaces. b) Top views of active sites on the CeO_2(111) and (110) surfaces (see text for details).

the ab initio adsorption energies of the stable Ce-end-on and Ce-parallel configurations (−11.4 and −11.9 kcal mol^{-1}, respectively) are consistent with that of −12.2 kcal mol^{-1} reported by Henderson et al.[38] and are slightly different from the values of −13.1–−14.1 kcal mol^{-1} measured by Prin et al.[39] In addition, the adsorption energies of the Ce-end-on and Ce-parallel configurations are in line with recent theoretical results of −12.9 and −13.4 kcal mol^{-1}, respectively, by Kumar and Schelling.[40] As summarized in Table 2, predicted geometrical parameters and vibrational frequencies of gas-phase H_2, OH, and H_2O in a 15 Å cubic box are in line with available experimental and theoretical data.

Table 2. Geometrical parameters and vibrational frequencies of gas-phase H_2, OH, and H_2O calculated by the DFT method.

Symmetry	H_2 $D_{\infty v}$		OH $C_{\infty v}$		H_2O C_{2v}	
	Calcd	Exptl[41]	Calcd	Exptl[42]	Calcd	Exptl[43,44]
r(O–H or H–H) [Å]	0.743	0.740	0.986	0.970	0.957	0.972
θ(H–O–H) [°]	–	–	–	–	104.5	104.7
ν_{asym} [cm^{-1}]	–	–	3642	3738	3856	3738
ν_{sym} [cm^{-1}]	4435	4400	–	–	3741	3436
ν_{bend} [cm^{-1}]	–	–	–	–	1585	1392

2.2. Location of Surface Intermediates

In order to initially locate possible intermediates, an H_2 molecule was placed on various CeO_2 surface sites as shown in Figure 4, where **I** and **II** correspond to the atop site of Ce and O atoms, respectively, while **III** and **IV** represent the bridging sites of Ce–Ce and O–O bonds, respectively. The atop site on a sublayer oxygen atom is represented by **V**. For the CeO_2(110) surface, **IV-S** and **IV-L** correspond to the short and long O–O bond-bridging sites, respectively. Furthermore, the H_2 molecule was placed both vertically and horizontally (Figure 4a) on each CeO_2 surface site—except the **V** conformation on CeO_2(111)—corresponding to **v** and **h**, respectively. Figures S1 and S2 (in the Supporting Information) display various adsorbed H_2 species on CeO_2(111) and (110). As compiled in Table S3, the adsorption energies of these adsorbed H_2 species on the (111) and (110) surfaces at the DFT and DFT+U levels are small, and the energy difference between the DFT and DFT+U methods for the stoichiometric surfaces is insignificant (< 0.3 kcal mol^{-1}). In particular, because the calculated energies are within the average bond-energy errors of the GGA method (≈2.0 kcal mol^{-1})[45] and to ensure the existence of initial intermediates for mechanistic studies on CeO_2(111) and (110), we carried out additional minimum-energy path (MEP) calculations at the DFT+U level using **II-v-(111)** and **IV-S-v-(110)** configurations with the lowest adsorption energy among intermediate states optimized on the (111) and (110) surfaces, respectively. Shown in Figure S3 are shallow wells with adsorption energies of approximately −0.5 and −1.4 kcal mol^{-1}, indicating that the **II-v-(111)** and **IV-S-v-(110)** configurations are van der Waals intermediates. It should be noted that the DFT method used in this study may not be suitable to describe long-range dispersion interactions (van der Waals interactions),[46] and to the best of our knowledge, van der Waals complexes for H_2–CeO_2 interactions have not been experimentally reported. However, we assume that these complexes are physisorbed intermediates,[47] which are adsorbed by molecular adsorption and connectable to chemisorbed local minima. These minima are related to dissociative adsorption processes, giving rise to LM2 and LM3 and LM5 and LM6 in Figures 5 and 6, to be discussed in the following section. Furthermore, to test the coverage effects of H_2–surface interactions, we compared 0.5- and 1.0-monolayer coverage using the **II-v-(111)** (LM1) configuration; the adsorption energy difference is negligible (≈0.1 kcal mol^{-1}).

2.3. Reaction Mechanisms

The decomposition of H_2 on CeO_2 may occur via a stepwise reaction mechanism, in which H_2 first adsorbs at a favorable active Ce^{4+} or O^{2-} site. Then, the adsorbed H_2 species directly dissociates, followed by the formation of OH species. Surface OH species can further diffuse on the reduced CeO_2 surface and interact with each other to produce H_2O, which is accom-

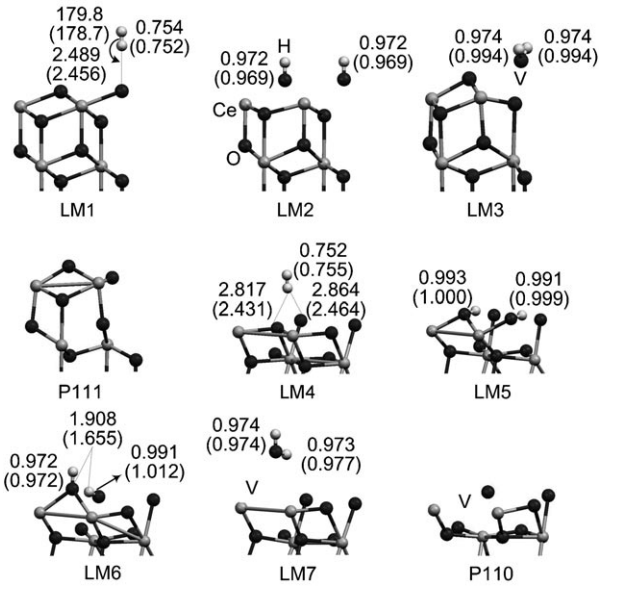

Figure 5. Optimized geometries with selected bond lengths [Å] and angles [°] of intermediates, transition states and products for the H_2–CeO_2 interactions. The values in parentheses are calculated by the DFT method; otherwise the values are from the DFT + U level.

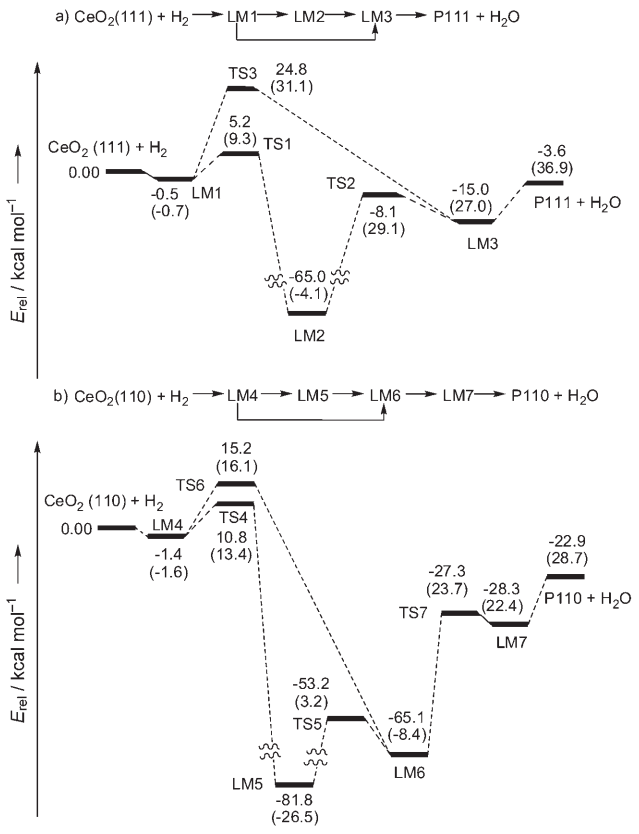

Figure 6. Reaction pathways for the reduction of a) CeO_2(111) and b) CeO_2(110) by H_2 along with corresponding schematic energy profiles for the H_2–CeO_2 interactions at the DFT + U level. The values in parentheses are those calculated by the DFT method.

panied by the reduction of Ce^{4+} to Ce^{3+} and the formation of an oxygen vacancy when H_2O desorbs.

We performed both the standard DFT and DFT + U calculations to map out the potential energy surfaces (PESs). Figure 5 and Figure S4 illustrate the geometries of optimized intermediates and products and transition states for the H_2 reactions on the CeO_2(111) and (110) surfaces, respectively, using the DFT and DFT + U methods. Compiled in Table 3 are the predicted relative energies at the DFT and DFT + U levels. These results

Table 3. Relative energies [kcal mol^{-1}] of the intermediates, transition states, and products of $CeO_2 + H_2$ interactions calculated at the DFT and DFT + U levels.

Species or reaction	DFT	DFT + U
$CeO_2(111) + O_2$	0.0	0.0
LM1	−0.7	−0.5
LM2	−4.1	−65.0
LM3	27.0	−15.0
TS1	9.3	5.2
TS2	29.1	−8.1
TS3	31.1	24.8
$P111 + H_2O$	36.9	−3.6
$CeO_2(110) + O_2$	0.0	0.0
LM4	−1.6	−1.4
LM5	−26.5	−81.8
LM6	−8.4	−65.1
LM7	22.4	−28.3
TS4	13.4	10.9
TS5	3.2	−53.2
TS6	16.1	15.2
TS7	23.7	−27.3
$P110 + H_2O$	28.7	−22.9

show that our calculated energetics, except for the initial intermediates LM1 and LM4, are significantly influenced by the inclusion of U–J, leading to different structural relaxations during H_2–surface interactions. In particular, to examine the energy difference between DFT and DFT + U, LDOS (local density of states) calculations for adsorbed hydrogen species and Ce and O ions on the top layer of the LM2 intermediate were performed. As illustrated in Figure S5, Ce 5d and Ce 4f states above the Fermi level may be a main factor for the large energy difference between DFT and DFT + U methods for the H_2–CeO_2 interactions. In the following, we will discuss mechanistic details based on the DFT + U results.

2.3.1. CeO_2(111) Reduction by H_2

The reduction of the CeO_2(111) surface by H_2 may occur according to the reaction pathway shown in Figure 6a. The initial interaction of the hydrogen molecule approaching the metal oxide surface is a van der Waals attraction, leading to LM1, **II-v-(111)**, with a physorsorption energy of 0.5 kcal mol^{-1}. In the optimized LM1 structure, the H–H distance is 0.754 Å, and the H–$O_{surface}$ distance is 2.489 Å. In the following step of the reaction, the LM1 complex has to overcome a 5.7 kcal mol^{-1} activation barrier for the dissociation process via **TS1**, producing the OH-containing LM2 intermediate with the equivalent O–H bonds of 0.972 Å. At **TS1**, the breaking H–H bond is 1.156 Å. The interaction of the two OH species in LM2 via **TS2** with a

high reaction barrier of ≈57 kcal mol^{-1} leads to the formation of a chemisorbed H_2O molecule in LM3, with an overall endothermicty of 50.0 kcal mol^{-1}. The breaking O–H bond and forming H–O bond in **TS2** are 2.908 Å and 1.288 Å, respectively. As mentioned above, Ce^{4+} cations can be reduced by the formation of H_2O species, and subsequently generating an oxygen vacancy (**V**, see Figure 5). The LM3 intermediate can also be formed by abstracting a surface oxygen via **TS3** with a high reaction barrier of 25.3 kcal mol^{-1}, bringing about concurrent O–H bond-forming and H–H bond-breaking processes with their corresponding bond lengths of 0.981 and 1.815 Å. This pathway is less favorable than the process via **TS1** due to its higher reaction barrier. Eventually, the LM3 intermediate can barrierlessly dissociate to produce P111 (Figure 5), and a gas-phase H_2O molecule with a 11.4 kcal mol^{-1} endothermicity, leading to nonstoichometric CeO_2 and an oxygen vacancy. The overall exothermicity of this process is 3.6 kcal mol^{-1} at the DFT + U level.

2.3.2. CeO_2(110) Reduction by H_2

Similar to LM1 on the CeO_2(111) surface, the H_2–CeO_2(110) complex, **IV-S-v-(110)**, (LM4) can be formed with a binding energy of 1.4 kcal mol^{-1} (Figure 6b). In the LM4 complex, the H–H distance is 0.752 Å, and the two H–O bonds are 2.817 and 2.864 Å. As summarized in the reaction pathway in Figure 6b, there are two possible pathways to produce P110 (Figure 5) and H_2O.

The surface H_2 species in LM4 can dissociate to generate the more stable OH-containing LM5 intermediate by overcoming an activation barrier of 12.3 kcal mol^{-1} at **TS4**. The breaking H–H bond length in **TS4** is 0.853 Å and the two O–H bonds in LM5 are essentially the same length (0.993 Å and 0.991 Å). One of the H atoms in LM5 can migrate to a neighboring O atom via **TS5** with a 28.6 kcal mol^{-1} barrier, thus producing LM6, which has a new O–H bond of 0.991 Å. The O–H bond lengths of LM6 (0.972 and 0.991 Å) are slightly different. The energetic difference between these two OH-containing intermediates, LM5 and LM6, stems from hydrogen bonding in these structures; there are two possibilities for hydrogen bonding with neighboring O atoms in LM5 but only one such possibility in LM6 (see Figure 5). In addition to the aforementioned reaction pathway, LM6 can also be formed directly via **TS6** with a reaction barrier of 16.6 kcal mol^{-1}. At **TS6**, the cleaving H–H bond is 0.812 Å, which is 0.06 Å longer than in LM4, indicating that **TS6** is an early transition state. The two OH groups in LM6 can interact to form LM7 through **TS7**, in which the H atom of the OH group lying parallel to the surface migrates to the OH group bonded perpendicular to the surface, generating a chemisorbed H_2O molecule and an oxygen vacancy with a reaction barrier of ≈38 kcal mol^{-1}. Finally, the weakly bound H_2O species in LM7 can desorb from the surface with an endothermicity of 5.4 kcal mol^{-1}. This process takes place with an overall exothermicity of 22.9 kcal mol^{-1} [about 19 kcal mol^{-1} lower than that of CeO_2(111)], producing P110 and H_2O.

MEP calculations clearly show that the reduction mechanism of CeO_2 by H_2 occurs via a stepwise reaction, as discussed above. The molecular-level interpretation using quantum chemical calculations supports the reaction mechanism proposed on the basis of experimental results.[9] For the reduction of CeO_2(111) by H_2, the predicted highest barrier, 25 kcal mol^{-1}, is in good agreement with the 27.5 kcal mol^{-1} activation energy reported by Al-Madfa et al.[48] A detailed rate-constant prediction based on the potential-energy profiles and experimental data will be carried out in the future.

2.4. Analysis of Vibrational Frequencies of Adsorbed OH and H_2O Species

Compiled in Table 4 is a summary of predicted vibrational frequencies of adsorbed OH (LM2, LM5, and LM6) and H_2O (LM3 and LM7) species at the DFT + U level. A variety of OH and H_2O species were observed using Fourier transform infrared (FTIR) spectroscopy.[49] It was reported that the bands at 3710, 3660, and 3600 cm^{-1} are attributed to one-, two- and three-coordinated configurations, respectively, of adsorbed OH species on CeO_2 surfaces, while those in the range of 3400–3450 cm^{-1} are related to H-bonded OH species.[49] The bands at 3686, 3140, and 1640 cm^{-1} and 3686, 3620, and 1595 cm^{-1} are assigned to a H-bonded and non-H-bonded H_2O species, respectively.[50] The calculated OH frequencies of LM2 (3641 and 3650 cm^{-1}) are consistent with the experimental value of 3600 cm^{-1} for the three-coordinated configuration of an adsorbed OH species and a theoretical result of 3627 cm^{-1} by Vicario and et al.[18] The calculated OH frequencies of LM5 (3258, and 3234 cm^{-1}) are slightly different from the theoretical value of 3100 cm^{-1},[18] assigned to an H-bonded OH species using experimental data[49] of 3400–3450 cm^{-1}. The predicted vibrational frequencies of the O–H stretching of LM6 (3636 and 3266 cm^{-1}) are close to those of H-bonded H_2O-like species (3686 and 3140 cm^{-1}).[50] Calculated vibrational frequencies corresponding to asymmetric, symmetric, and bending modes of the H_2O-like species of LM3 (3657, 3605, 1535 cm^{-1}, respectively) are in line with experimental values (3686, 3620, 1595 cm^{-1}, respectively),[50] while the frequencies found for LM7 (3814, 3694, and 1591 cm^{-1}) are close to those of a gas-phase H_2O molecule (Table 2), implying that LM7 has more product character than LM3.

Table 4. Predicted vibrational frequencies of OH or H_2O species on CeO_2.[a]

Surface	Intermediate	Adsorbed species	This work [cm^{-1}]	Literature[18] [cm^{-1}]
(111)	LM2	OH	3641, 3650	3627
(111)	LM3	H_2O	3657, 3605, 1535	–
(110)	LM5	OH	3258, 3234	3100
(110)	LM6	OH	3636, 3266	–
(110)	LM7	H_2O	3814, 3694, 1591	–

[a] Calculated by the DFT + U method.

3. Conclusions

The reduction mechanisms of the CeO_2(111) and (110) surfaces by H_2 have been elucidated using periodic DFT and DFT+U calculations. The validity of the surface models was verified by estimating various properties, such as the lattice parameters, total density of states of bulk CeO_2, the formation energy of an oxygen vacancy, adsorption energies of H_2O on CeO_2(111), and the surface stability of CeO_2(111) and (110), in line with available literature data. For the mechanistic studies, molecular and dissociative local minima were initially located by placing an H_2 molecule at various active sites on each CeO_2 surface. The adsorption energies of the DFT and DFT+U methods of these molecular adsorption intermediates are small, whereas the dissociative adsorption processes producing hydroxylated surfaces are energetically favored, with exothermicity increasing from 65.0 kcal mol^{-1} on the (111) surface to 81.8 kcal mol^{-1} on the (110) surface. The DFT+U methodology produced more accurate energetics, especially on the reduced ceria surfaces. The potential-energy profiles for these surface reactions have been constructed by mapping out their MEPs using the NEB method. The intermediates of the molecular and dissociative adsorption on each CeO_2 surface were connected by the NEB method with well-defined transition states. It was found that the reduction of the CeO_2 surface takes place via a stepwise mechanism: adsorption/dissociation of H_2 with the formation of OH species and desorption of H_2O along with the reduction of Ce^{4+} and the formation of an oxygen vacancy. According to the MEP calculations, the less stable (110) surface is energetically more favorable. Our estimated vibrational frequencies of adsorbed OH and H_2O species agree well with available experimental and theoretical results.

Acknowledgements

We acknowledge the use of CPU's from National Center for High-Performance Computing, Taiwan, supported by INER under contract No. NL 940251. M.C.L. also wants to acknowledge the support from the MOE ATP program, Taiwan Semiconductor Manufacturing Co. for the TSMC Distinguished Professorship and Taiwan National Science Council for the Distinguished Visiting Professorship at the Center for Interdisciplinary Molecular Science, National Chiao Tung University, Hsinchu, Taiwan. We greatly appreciate the reviewer's valuable comments and suggestions.

Keywords: density functional calculations · reaction mechanisms · reduction · surface chemistry · vibrational spectroscopy

[1] A. F. Diwell, R. R. Rajaram, H. A. Shaw, T. J. Treux, *The role of ceria in three-way catalysts, in Catalysis Automotive Pollution Control, Vol. 71* (Ed.: A. Cruq), Elsevier, Amsterdam, **1991**.
[2] H. C. Yao, Y. F. Y. Yao, *J. Catal.* **1984**, *86*, 254.
[3] a) L. Kundakovic, M. Flytzani-Stephanopoulos, *J. Catal.* **1998**, *179*, 203; b) M. J. Tiernan, O. E. Finlayson, *Appl. Catal. B* **1998**, *19*, 23.
[4] J. Stubenrauch, J. M. Vohs, *J. Catal.* **1996**, *159*, 50.
[5] a) W. Liu, M. Flytzani-Stephanopoulos, *J. Catal.* **1995**, *153*, 317; b) W. Liu, M. Flytzani-Stephanopoulos, *J. Catal.* **1995**, *153*, 304.
[6] a) H. Idriss, C. Diagne, J. P. Hindermann, A. Kiennemann, M. A. Barteau, *J. Catal.* **1995**, *155*, 219; b) M. I. Zaki, M. A. Hasan, L. Pasupulety, *Langmuir* **2001**, *17*, 768.
[7] a) Y. Liu, S. Zha, M. Liu, *Chem. Mater.* **2004**, *16*, 3502; b) C. Xia, M. Liu, *Solid State Ionics* **2002**, *152–153*, 423; c) C. Xia, Y. Zhang, M. L. Liu, *Electrochem. Solid-State Lett.* **2003**, *6*, A290; d) S. Zha, A. Moore, H. Abernathy, M. Liu, *J. Electrochem. Soc.* **2004**, *151*, A1128; e) S. Zha, W. Rauch, M. Liu, *Solid State Ionics* **2004**, *166*, 241.
[8] a) K. Huang, M. Feng, J. B. Goodenough, *J. Am. Ceram. Soc.* **1998**, *81*, 357; b) B. C. Morris, W. R. Flavell, W. C. Mackrodt, M. A. Morris, *J. Mater. Chem.* **1993**, *3*, 1007; c) L. Navarro, F. Marques, J. Frade, *J. Electrochem. Soc.* **1997**, *144*, 276; d) K. M. Ryan, J. P. McGrath, R. A. Farrell, W. M. O'Neill, C. J. Barnes, M. A. Morris, *J. Phys. Condens. Matter* **2003**, *15*, L49; e) H. L. Tuller, A. S. Nowick, *J. Electrochem. Soc.* **1976**, *123*, 209; f) B. Zhu, X. Luo, C. Xia, I. Albinsson, B. F. Mellander, *Ionics* **1997**, *3*, 263; g) W. M. O'Neill, M. A. Morris, *Chem. Phys. Lett.* **1999**, *305*, 389.
[9] E. Aneggi, M. Boaro, C. de Leitenburg, G. Dolcetti, A. Trovarelli, *J. Alloys Compd.* **2006**, *408*, 1096.
[10] L. A. Bruce, M. Hoang, A. E. Hughes, T. W. Turney, *Appl. Catal. A* **1996**, *134*, 351.
[11] a) C. Lamonier, A. Ponchel, A. D'Huysser, L. Jalowiecki-Duhamel, *Catal. Today* **1999**, *50*, 247; b) C. Padeste, N. W. Cant, D. L. Trimm, *Catal. Lett.* **1993**, *18*, 305; c) V. Perrichon, A. Laachir, G. Bergeret, R. Fréty, L. Tournayan, O. Touret, *J. Chem. Soc. Faraday Trans.* **1994**, 773; d) G. Wrobel, C. Lamonier, A. Bennani, A. D'Huysser, A. Aboukais, *J. Chem. Soc. Faraday Trans.* **1996**, 2001.
[12] a) J. L. G. Fierro, S. Mendioroz, A. O. Olivan, *J. Colloid Interface Sci.* **1985**, *107*, 60; b) J. L. G. Fierro, J. Soria, J. Sanz, J. M. Rojo, *J. Solid State Chem.* **1987**, *66*, 154.
[13] S. Bernal, J. J. Calvino, G. A. Cifredo, J. M. Gatical, J. A. Pérez Omil, J. M. Pintado, *J. Chem. Soc. Faraday Trans.* **1993**, 3499.
[14] S. Gennard, F. Corà, C. R. A. Catlow, *J. Phys. Chem. B* **1999**, *103*, 10158.
[15] Y. Jiang, J. B. Adams, M. V. Schilfgaarde, *J. Chem. Phys.* **2005**, *123*, 064701.
[16] N. V. Skorodumova, M. Baudin, K. Hermansson, *Phys. Rev. B* **2004**, *69*, 075401.
[17] N. V. Skorodumova, S. I. Simak, B. I. Lundqvist, I. A. Abrikosov, B. Johansson, *Phys. Rev. Lett.* **2002**, *89*, 166601.
[18] G. Vicario, G. Balducci, S. Fabris, S. de Gironcoli, S. Baroni, *J. Phys. Chem. B* **2006**, *110*, 19380.
[19] Z. Yang, T. K. Woo, M. Baudin, K. Hermansson, *J. Chem. Phys.* **2004**, *120*, 7741.
[20] Z. Yang, T. K. Woo, K. Hermansson, *J. Chem. Phys.* **2006**, *124*, 224704.
[21] a) V. I. Anisimov, J. Zaanen, O. K. Anderson, *Phys. Rev. B* **1991**, *44*, 943; b) S. L. Dudarev, G. A. Botton, S. Y. Savrasov, C. J. Humphreys, A. P. Sutton, *Phys. Rev. B* **1998**, *57*, 1505.
[22] M. Nolan, S. Grigoleit, D. C. Sayle, S. C. Parker, G. W. Watson, *Surf. Sci.* **2005**, *576*, 217.
[23] M. Nolan, S. C. Parker, G. W. Watson, *Surf. Sci.* **2005**, *595*, 223.
[24] a) G. Kresse, J. Furthmüller, *Phys. Rev. B* **1996**, *54*, 11169; b) G. Kresse, J. Hafner, *Phys. Rev. B* **1993**, *47*, 558.
[25] P. Blochl, *Phys. Rev. B* **1994**, *17*, 953.
[26] a) Y. M. Choi, H. Abernathy, H.-T. Chen, M. C. Lin, M. Liu, *ChemPhysChem* **2006**, *7*, 1957; b) For an initial study, we did not carry out the DFT+U approach. To precisely characterize the partially reduced CeO_2 surface, we have examined the oxygen-reduction mechanism on a CeO_2(111) surface by using the DFT+U methodology, which will be reported.
[27] H. J. Monkhorst, J. D. Pack, *Phys. Rev. B* **1976**, *13*, 5188.
[28] W. Hayes, *Crystals with the Fluorite Structure*, Clarendon, Oxford, **1974**.
[29] DFT and DFT+U correspond to GGA-PAW-DFT and GGA-PAW-DFT+ U, respectively.
[30] a) G. Henkelman, B. P. Uberuaga, H. Jönsson, *J. Chem. Phys.* **2000**, *113*, 9901; b) G. Mills, H. Jönsson, G. Schenter, *Surf. Sci.* **1995**, *324*, 305.
[31] N. V. Skorodumova, R. Ahuja, S. I. Simak, I. A. Abrikosov, B. Johansson, B. I. Lundqvist, *Phys. Rev. B* **2001**, *64*, 115108.
[32] S. E. Hill, C. R. A. Catlow, *J. Phys. Chem. Solids* **1993**, *54*, 411.
[33] E. A. Kummerle, G. Heger, *J. Solid State Chem.* **1999**, *147*, 485.
[34] Y.-M. Chiang, E. B. Lavik, D. A. Blom, *Nanostruct. Mater.* **1997**, *9*, 663.
[35] a) D. M. Lyons, J. P. McGrath, M. A. Morris, *J. Phys. Chem. B* **2003**, *107*, 4607; b) D. M. Lyons, K. M. Ryan, M. A. Morris, *J. Mater. Chem.* **2002**, *12*, 1207.

[36] M. Baudin, M. Wojcik, K. Hermansson, *Surf. Sci.* **2000**, *468*, 51 (see Supporting Information).
[37] J. C. Conesa, *Surf. Sci.* **1995**, *339*, 337 (see Supporting Information).
[38] M. A. Henderson, C. L. Perkins, M. H. Engelhard, S. Thevuthasan, C. H. F. Peden, *Surf. Sci.* **2003**, *526*, 1.
[39] M. Prin, M. Pijolat, M. Soustelle, O. Touret, *Thermochim. Acta* **1991**, *186*, 273.
[40] S. Kumar, P. K. Schelling, *J. Chem. Phys.* **2006**, *125*.
[41] *CRC Handbook of Chemistry and Physics, 76th ed.*, CRC, New York, **1996**.
[42] S. P. Walch, C. M. Rohlfing, C. F. Melius, C. W. Bauschlicher Jr, *J. Chem. Phys.* **1988**, *88*, 6273.
[43] C. W. Kern, M. Karplw, *Water: A Comprehensive Treatise*, Plenum, New York, **1972**.
[44] B. J. Rosenberg, W. C. Ermler, I. Shavitt, *J. Chem. Phys.* **1976**, *65*, 4072.
[45] W. Kohn, A. D. Becke, R. G. Parr, *J. Phys. Chem.* **1996**, *100*, 12974.
[46] S. Kristyán, P. Pulay, *Chem. Phys. Lett.* **1994**, *229*, 175.
[47] a) K. J. Laidler, *Chemical Kinetics, 3rd ed.*, Benjamin Cummings, Massachusetts, **1997**; b) Physisorption and chemisorption can be distinguished by adsorption energies, that is, less than 4.8 kcal mol^{-1} and 70–120 kcal mol^{-1}, respectively.
[48] a) H. A. Al-Madfa, M. M. Khader, *Mater. Chem. Phys.* **2004**, *86*, 180; b) H. A. Al-Madfa, M. M. Khader, M. A. Morris, *Int. J. Chem. Kinet.* **2004**, *36*, 293.
[49] a) A. Badri, C. Binet, J. C. Lavalley, *J. Chem. Soc. Faraday Trans.* **1996**, 4669; b) C. Binet, M. Daturi, J. C. Lavalley, *Catal. Today* **1999**, *50*, 207; c) A. Laachir, V. Perrichon, A. Badri, J. Lamotte, E. Catherine, J. C. Lavalley, J. El Fallah, L. Hilaire, F. Le Normand, E. Quéméré, G. N. Sauvion, O. Touret, *J. Chem. Soc. Faraday Trans.* **1991**, 1601.
[50] M. Daturi, E. Finocchio, C. Binet, J. C. Lavalley, F. Fally, V. Perrichon, *J. Phys. Chem. B* **1999**, *103*, 4884.

Received: September 21, 2006
Revised: February 15, 2007
Published online on March 21, 2007

